Serrulatane diterpenoids from the leaves of Eremophila glabra and their potential as antihyperglycemic drug leads

Petersen, Malene J.; Liang, Chao; Kjaerulff, Louise; Ndi, Chi; Semple, Susan; Buirchell, Bevan; Coriani, Sonia; Møller, Birger Lindberg; Staerk, Dan

Published in:
Phytochemistry

Link to article, DOI:
10.1016/j.phytochem.2021.113072

Publication date:
2022

Document Version
Publisher's PDF, also known as Version of record

Phytochemistry 196 (2022) 113072

Contents lists available at ScienceDirect

Phytochemistry

journal homepage: www.elsevier.com/locate/phytochem

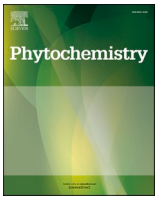

Serrulatane diterpenoids from the leaves of *Eremophila glabra* and their potential as antihyperglycemic drug leads

Malene J. Petersen [a], Chao Liang [a], Louise Kjaerulff [a], Chi Ndi [b], Susan Semple [b], Bevan Buirchell [c], Sonia Coriani [d], Birger Lindberg Møller [e], Dan Staerk [a,*]

[a] Department of Drug Design and Pharmacology, Faculty of Health and Medical Sciences, University of Copenhagen, Universitetsparken 2, DK-2100, Copenhagen, Denmark
[b] Quality Use of Medicines and Pharmacy Research Centre, Clinical and Health Sciences, University of South Australia, Frome Road, Adelaide, 5000, Australia
[c] Wise Owl Consulting, Como, Western Australia, 6152, Australia
[d] Department of Chemistry, Technical University of Denmark, Kemitorvet Building 207, DK-2800, Kongens Lyngby, Denmark
[e] Plant Biochemistry Laboratory, Department of Plant and Environment Sciences, University of Copenhagen, Thorvaldsensvej 40, DK-1871, Frederiksberg C, Denmark

ARTICLE INFO

Keywords:
Eremophila glabra
Scrophulariaceae
High-resolution inhibition profiling
Serrulatane diterpenoids
Flavonoids
Protein-tyrosine phosphatase 1B
α-Glucosidase

ABSTRACT

Eremophila (Scrophulariaceae) is a genus of Australian desert plants, which have been used by Australian Aboriginal people for various medicinal purposes. Crude extracts of the leaf resin of *Eremophila glabra* (R.Br.) Ostenf. showed α-glucosidase and protein tyrosine phosphatase 1B (PTP1B) inhibitory activity with IC_{50} values of 19.3 ± 1.2 μg/mL and 11.8 ± 2.1 μg/mL, respectively. Dual α-glucosidase/PTP1B high-resolution inhibition profiling combined with HPLC-PDA-HRMS and NMR were used to isolate and identify the compounds providing these activities. This resulted in isolation of seven undescribed serrulatane diterpenoids, eremoglabrane A-G, together with nine previously identified serrulatane diterpenoids and flavonoids. Three of the serrulatane diterpenoids showed PTP1B inhibitory activities with IC_{50} values from 63.8 ± 5.8 μM to 104.5 ± 25.9 μM.

1. Introduction

Natural products (NPs) continue to be a treasure chest in the hunt for new drug leads. NPs are characterized by a high diversity and structural complexity, and the traditional use of plant extracts can be helpful in the determination of which plants to investigate (Atanasov et al., 2021). As reviewed by Newman and Cragg (2020), around 38% of all approved small-molecule drugs in the period 1981–2019 were either of natural origin, derived from NPs, or synthetic drugs based on NP pharmacophores, showing that NPs continue to directly contribute to and to inspire the development of new drug leads.

The traditional use of plants in the *Eremophila* genus has led to the search for bioactive compounds in the more than 200 identified species (Ghisalberti, 1994). *Eremophila* belongs to the family Scrophulariaceae (figworts) and is endemic to Australia. *Eremophila* exhibits an immense morphological diversity throughout the Eremean (arid) biome, which covers approximately 70% of the Australian continent, being tolerant to extreme weather conditions, such as drought, fire or cold. *Eremophila glabra* (R.Br.) Ostenf. (tar bush) is widespread and grows in a wide range of soils and vegetation associations, although only in the drier areas of the continent (Brown and Buirchell, 2011).

Plants of the *Eremophila* genus are rich in terpenoids, polyphenols, fatty acids, verbascosides, and lignans (Singab et al., 2013). Some of the major NPs are the diterpenoids, including serrulatane, eremane, viscidane, decipiane, and cembrene types. Within the diterpenoids, serrulatane diterpenoids are by far the most abundant (Forster et al., 1986; Algreiby et al., 2018). Several bioactivities have been associated with *Eremophila*, spp., including antibacterial, antiviral, and antidiabetic activities (Semple et al., 1998; Ndi et al., 2007; Smith et al., 2007; Tahtah et al., 2016; Wubshet et al., 2016; Algreiby et al., 2018; Kjaerulff et al.,

Abbreviations: Bis-Tris, bis(2-hydroxyethyl)amino-tris(hydroxymethyl)methane; COSY, correlation spectroscopy; DMSO, dimethyl sulfoxide; DTT, dithiothreitol; ECD, electronic circular dichroism; EDTA, *N,N,N′,N′*-ethylenediaminetetraacetate; HMBC, heteronuclear multiple-bond correlation; HPLC, high-performance liquid chromatography; HRMS, high-resolution mass spectrometry; HSQC, heteronuclear single quantum coherence; NMR, nuclear magnetic resonance; NOE, nuclear Overhauser effect; PDA, photodiode array; *p*-NPG, *p*-nitrophenyl α-D-glucopyranoside; *p*-NPP, *p*-nitrophenyl phosphate; PTP1B, protein-tyrosine phosphatase 1B; ROESY, rotating frame Overhauser effect spectroscopy; T2D, type 2 diabetes; Tris, tris(hydroxymethyl)-aminomethane.

* Corresponding author.
E-mail address: ds@sund.ku.dk (D. Staerk).

https://doi.org/10.1016/j.phytochem.2021.113072
Received 25 October 2021; Received in revised form 21 December 2021; Accepted 24 December 2021
Available online 29 December 2021

2020; Pedersen et al., 2020), and it is thus a promising source for identification of new bioactive compounds.

Diabetes is a multiparametric metabolic disorder, and the global prevalence of diabetes in the 20–79-year age group was estimated to be around 463 million in 2019 (International Diabetes Federation, 2019). The number of cases is estimated to increase to around 700 million by 2045, causing an estimated similar increase in the 760 billion USD global health care expenditures encountered in 2019. These figures serve to emphasise the future challenges of providing adequate health care worldwide. Approximately 90% of all diabetes cases are caused by type 2 diabetes (T2D). T2D is characterized by insufficient insulin production by the pancreatic β-cells and/or insulin resistance in target organs like the liver, muscles, and fat tissue (Chatterjee et al., 2017). This leads to hyperglycaemia, which, if left untreated, results in long-term complications like nephropathy, neuropathy, retinopathy, and cardiovascular diseases. T2D is strongly associated with a sedentary lifestyle and obesity. Currently available treatment of T2D includes, in addition to medication, a combination of increased physical exercise and changed dietary habits, aiming at maintaining a lowered and stable blood glucose. α-Glucosidase is an enzyme present in the small intestine, where it catalyses hydrolysis of (1 → 4)-linked α-D-glucose residues from the terminal non-reducing ends of primarily disaccharides, trisaccharides, and oligosacchrides into absorbable monosaccharides. Inhibition of α-glucosidase therefore lowers the postprandial blood glucose levels, and acarbose, voglibose, and miglitol have been approved as drugs inhibiting α-glucosidase (Padhi et al., 2020), but are associated with a series of side effects. Therefore, new and improved α-glucosidase inhibitors are in demand. Protein tyrosine phosphatase 1B (PTP1B) is a protein tyrosine phosphatase catalyzing dephosphorylation of tyrosine residues of the insulin receptor kinase, and hereby down-regulating insulin signalling (Galic et al., 2005). Studies have furthermore shown that PTP1B affects peptidic hunger hormon leptin signalling and that mice lacking PTP1B are resistant to obesity as well as being more sensitive to insulin (Zabolotny et al., 2002). Inhibition of PTP1B thus appear to be a promising way of treating T2D and potentially also to prevent obesity. No drugs with PTP1B inhibitory activity are on the market, but several studies have identified diterpenoids as effective PTP1B inhibitors in vitro (Hjortness et al., 2018; Wubshet et al., 2016; Kjaerulff et al., 2020), and thus future potential drugs for treatment of T2D and obesity. *E. glabra* is positioned in the resin-accumulating phylogenetic clade H14, known to accumulate serrulatane diterpenoids (Gericke et al., 2021), and was therefore selected as our target species in our search for new drug leads with potential antidiabetic properties.

2. Results and discussion

As part of our ongoing investigation of plants for antihyperglycaemic activity, a crude acetonitrile leaf resin extract of *E. glabra* (R.Br.) Ostenf. was assessed for α-glucosidase and PTP1B inhibitory activity and provided IC_{50} values of 19.3 ± 1.2 μg/mL and 11.8 ± 2.1 μg/mL, respectively (Supplementary data Fig. S36). The extract was therefore further investigated to pinpoint the individual constituents responsible for the observed inhibitory activities.

2.1. High-resolution inhibition profiling of the crude resin extract and isolation of selected compounds

To identify individual constituents responsible for the observed bioactivities, the crude resin extract was fractionated using analytical-scale high-performance liquid chromatography (HPLC) and the eluate from 20 to 60 min was microfractionated into two sets of two 96-well microplates. The content in each well was assayed, and the results expressed as percentage α-glucosidase and PTP1B inhibition were plotted at the respective retention times to provide the dual high-resolution α-glucosidase/PTP1B inhibition profile shown in Fig. 1.

The peaks and/or fractions 5, 7, 8, 10, 12, and 13 (Fig. 1) were correlated with α-glucosidase inhibitory activity, whereas a few peaks within the retention time range 45–55 min were correlated with PTP1B inhibitory activity. Each of the peaks/fractions were collected by the use of semi-preparative scale HPLC and further purified using analytical-scale HPLC. This afforded 0.33 mg of **1**, 1.03 mg of **2**, 2.39 mg of **3**, 1.23 mg of **4,** 0.33 mg of **5a**, 0.24 mg of **5b**, 0.21 mg of **5c**, 3.19 mg of **6**, 0.68 mg of **7,** 0.84 mg of **8a**, 0.37 mg of **8b**, 2.04 mg of **9**, 0.23 mg of **10b**, 1.95 mg of **11**, 0.24 mg of **12b**, and 0.40 mg of **13c**.

By comparison of the NMR data obtained with those reported in the literature, compound **1** was identified as hispidulin (Botirov and Karimov, 2018), **2** as jaceosidin (Reinhardt et al., 2019), **3** as pectolinarigenin (Zahran et al., 2019), **4** as eupatilin (Reinhardt et al., 2019), **5b** as 18-acetoxy-8,20-dihydroxyserrulat-14-en-19-oic acid (Algreiby et al., 2018), **6** as 8,20-dihydroxyserrulat-14-en-19-oic acid (Forster et al., 1986), **9** as 20-acetoxy-8-hydroxyserrulat-14-en-19-oic acid (Ndi et al., 2007), **11** as 8,20-diacetoxyserrulat-14-en-19-oic acid (Forster et al., 1986), and **12b** as serrulat-14-ene-7,8,20-triol (Croft et al., 1981). ^{1}H-NMR data of these constituents are provided in Supplementary data Table S1. The remaining compounds were identified as previously unreported serrulatane diterpenoids (Fig. 2).

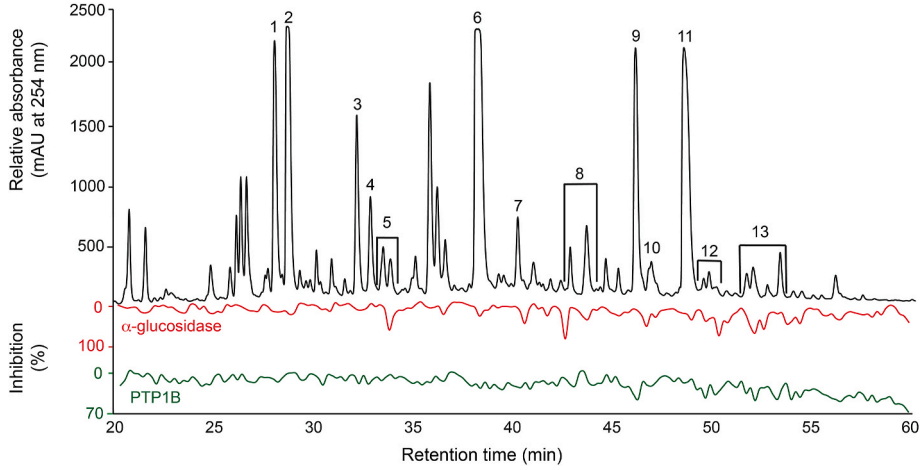

Fig. 1. Dual high-resolution α-glucosidase/PTP1B inhibition profile of the crude extract of *E. glabra* leaf resin. The analytical-scale HPLC profile recorded at 254 nm is shown at the top with isolated fractions/compounds marked by numbers. The corresponding high-resolution α-glucosidase (red) and PTP1B (green) inhibition profiles are shown below. (For interpretation of the references to colour in this figure legend, the reader is referred to the Web version of this article.)

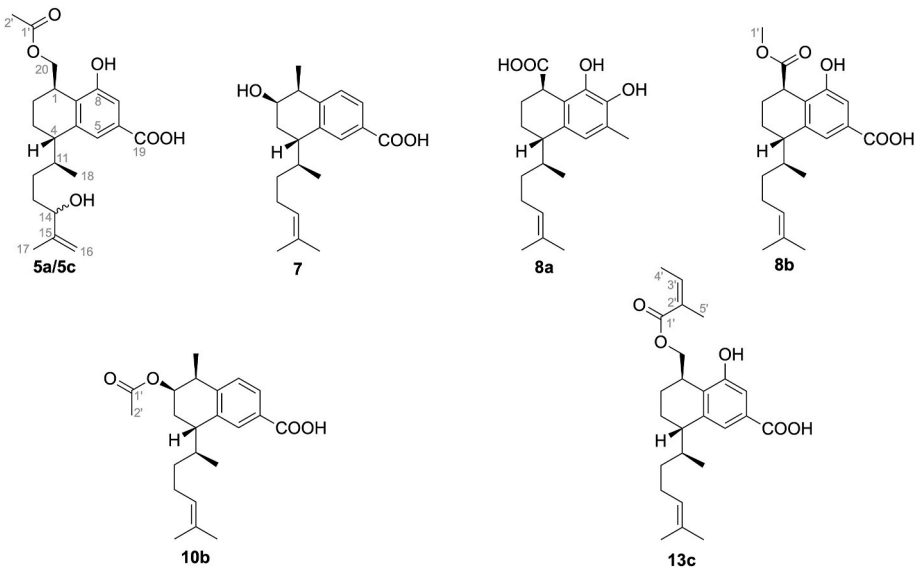

Fig. 2. Structures of previously unreported serrulatane-type diterpenoids isolated from leaves of *E. glabra*. The full chemical names of the compounds **5a**, **5c**, **7**, **8a**, **8b**, **10b**, and **13c** are found in the main text.

2.2. Structure elucidation of previously undescribed natural products

The constituent collected as peak **7** showed an $[M+H]^+$ ion at *m/z* 317.2109 (calcd. 317.2111, ΔM +0.7) suggesting the molecular formula $C_{20}H_{28}O_3$, which corresponds to a hydrogen deficiency index of 7. The 1D ^{1}H NMR data showed signals for a 1,2,4 trisubstituted benzene moiety at δ_H 7.99 (br d, $J_{H5,H7} = 1.7$ Hz, H-5), δ_H 7.87 (dd, $J_{H7,H8} = 8.1$ Hz, $J_{H5,H7} = 1.7$ Hz, H-7), and δ_H 7.32 (dd, $J_{H7,H8} = 8.1$ Hz, $J_{H1,H8} = 0.6$ Hz, H-8). The COSY spectrum showed correlations corresponding to a H_3-20 ↔ H-1 ↔ H-2 ↔ H_2-3 ↔ H-4 ↔ H-11(H_3-18) ↔ H_2-12 ↔ H_2-13 ↔ H-14 ↔ H_3-16/H_3-17 spin system (Fig. 3), the latter being due to long-range couplings, suggesting the presence of a serrulat-14-en-19-oic acid core moiety. The carboxylic acid positioned at C-6 was confirmed by HMBC correlations from H-5 and H-7 to C-19, and the presence of a hydroxyl group at C-2 was inferred from the down field shift of oxymethine H-2 (δ_H 4.20, δ_C 69.9) as well as the remaining OH group to match the molecular formula. The 2D ROESY spectrum revealed a ROE correlation between H-4 and H-20, indicating them to be on the same plane of the molecule, and thus tentatively assigned the 1*S**,4*S** configuration as shown in Fig. 3.

Likewise, ROE correlations between H-5 and H-11, between H-4 and H_3-18, and between H3α and H_2-12 suggest the 11*S** configuration. The hydroxyl group at C-2 was assigned the β-orientation based on a strong ROE correlation between H-1 and H-2 and weaker ROE correlations between H-2 and H_3-20, H-3α, H-3β, and H_2-12. Finally, H_3-16 and H_3-17 were assigned based on ROE correlations to H-14 and H_2-13, respectively. The absolute configurations at C-1, C-4, and C-11 in serrulatanes isolated from *Eremophila* spp. have previously been established by comparison of experimental and calculated ECD spectra (Kumar et al., 2018 and unpublished result from our own lab). In addition to that, it has recently been proposed that serrulatane diterpenoids originate from the same 8,9-dihydroserrulat-14-ene precursor containing a basic serrulatane skeleton derived from nerylneryldiphosphate (Gericke et al., 2020), and it can therefore be assumed that the stereochemistry at

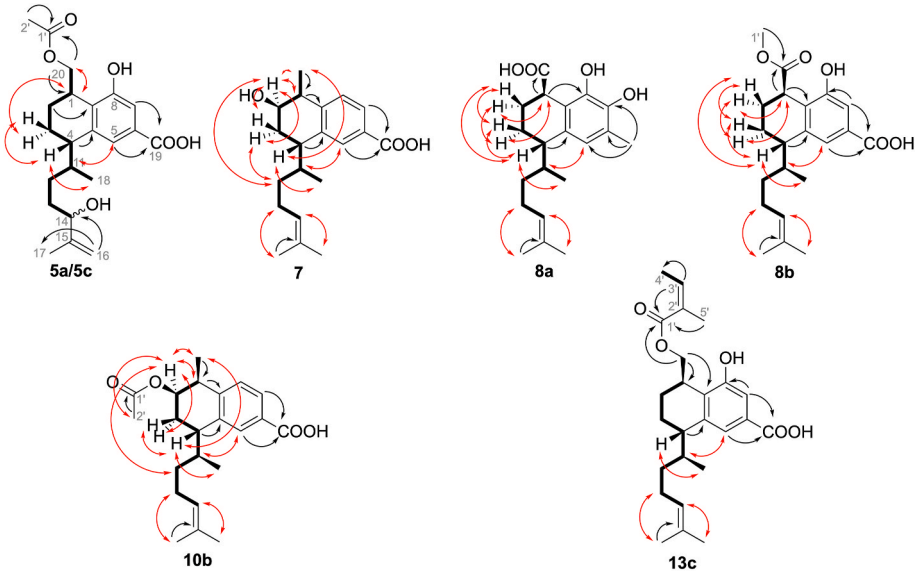

Fig. 3. Key COSY (bold), HMBC (black, H to C), and ROESY (red) correlations used for structure elucidation of the previously unreported serrulatane-type diterpenoids isolated from *E. glabra*. (For interpretation of the references to colour in this figure legend, the reader is referred to the Web version of this article.)

C1, C-4, and C-11 is preserved in naturally occurring serrulatanes produced by plants of the Scrophulariaceae family. Compound **7** is thus tentatively assigned the 1*S*,2*R*,4*S*,11*S* configuration. Comparison of calculated and experimental ECD spectra was subsequently used to substantiate this configurational assignment. Thus, experimental ECD spectra of all isolated serrulatane diterpenoids were grouped according to structural similarities, with ECD spectra of compounds with a carboxylic acid at C-19 and a hydroxyl group at C-8 in group A, compounds with hydroxyl groups at both C-7 and C-8 in group B, and compounds with a carboxylic acid at C-19 in group C (Fig. 4A–C). ECD calculations were subsequently performed using one model structure for each group (Fig. 4D–F), with a model structure for **5a** from group A, a model structure for **8a** from group B, and a model structure for **7** from group C.

To reduce the computational cost due to the high flexibility of the side chain at C-4, model compounds without C-14 to C-17, which has no significant effect on the ECD spectrum, were used for the quantum chemical calculations. Thus, the **7-model** shown in Fig. 4F were used for calculation of ECD spectra of **7**. Conformational search for the 3D structure of (1*S*,2*R*,4*S*,11*S*)-**7 model** led to 64 possible conformers, among which the 12 dominant ones with more than 1% of the Boltzmann population were used for calculation of ECD spectra (Supplementary data Tables S11 and S12). The experimental ECD spectrum of **7**, characterized by a negative and positive band around 215 and 235 nm, respectively, overall matched the calculated spectrum (Fig. 4F). However, it should be noted that the intensity of the negative Cotton effect at 215 nm in the calculated ECD spectrum is by far weaker than that in the experimental spectrum, which could be explained using a truncated structure of **7** for the performed ECD calculations. Thus, compound **7** was identified as (1*S*,2*R*,4*S*,11*S*)-2-hydroxyserrulat-14-en-19-oic acid, which has not previously been reported and for which the name eremoglabrane C is suggested. ^{1}H and ^{13}C NMR data are provided in Table 1, selected 2D NMR correlations are shown in Fig. 3, ^{1}H and ^{13}C NMR data and all correlations from 2D NMR experiments are provided in Supplementary data Table S4, and ^{1}H NMR, COSY, HSQC, HMBC and ROESY spectra are provided in Supplementary data Figs. S11–S15.

The constituents collected as peak **5a** and **5c** showed $[M+H]^+$ ions at *m/z* 391.2111 (calcd. 391.2115, ΔM +1.1) and 391.2105 (calcd. 391.2115, ΔM +2.6), respectively, suggesting a molecular formula of $C_{22}H_{30}O_6$ for both compounds, which corresponds to a hydrogen deficiency index of 8. The 1D ^{1}H NMR data of **5a** and **5c** revealed signals for the two meta-coupled aromatic protons H-5 and H-7, and the COSY spectrum showed correlations corresponding to a H_2-20 ↔ H-1 ↔ H_2-2 ↔ H_2-3 ↔ H-4 ↔ H-11(H_3-18) ↔ H_2-12 ↔ H_2-13 ↔ H-14 spin system. These data were in agreement with that of the previously reported **9**, with an acetoxylation at C-20. However, **5a** and **5c** differed from **9** by not having the characteristic olefinic triplet of septets for the 14-ene structure. Instead aliphatic oxymethine signals were observed at δ_H 3.87 (dd, $J_{H13B,H14}$ = 7.4 Hz, $J_{H13A,H14}$ = 6.5 Hz, H-14, δ_C 76.6) for **5a** and at δ_H 3.86 (t, $J_{H13B,H14} = J_{H13A,H14}$ = 6.7 Hz, H-14, δ_C 77.2) for **5c**, showing the presence of a hydroxyl group at C-14. A geminal pair of vinylic protons appeared at δ_H 4.72 and δ_H 4.83 (H-16A, H-16B, δ_C 110.8) for **5a** and at δ_H 4.72 and δ_H 4.77 (H-16A, H-16B, δ_C 111.4) for **5c** which both showed COSY correlations to H-17 and HMBC correlations to C-14 and C-17, suggesting a double bond between C-15 and C-16. The 2D ROESY spectra showed that both **5a** and **5c** exhibited the same relative configuration at C-1, C-4, and C-11 (Fig. 3), consistent with all other serrulatanes isolated in this work. The fact that these two compounds show almost identical NMR spectra suggests them to be epimers, and since the configuration at C-1, C-4 and C-11 are identical, they must be epimers at C-14. This was also suggested by ROESY data, since H-14

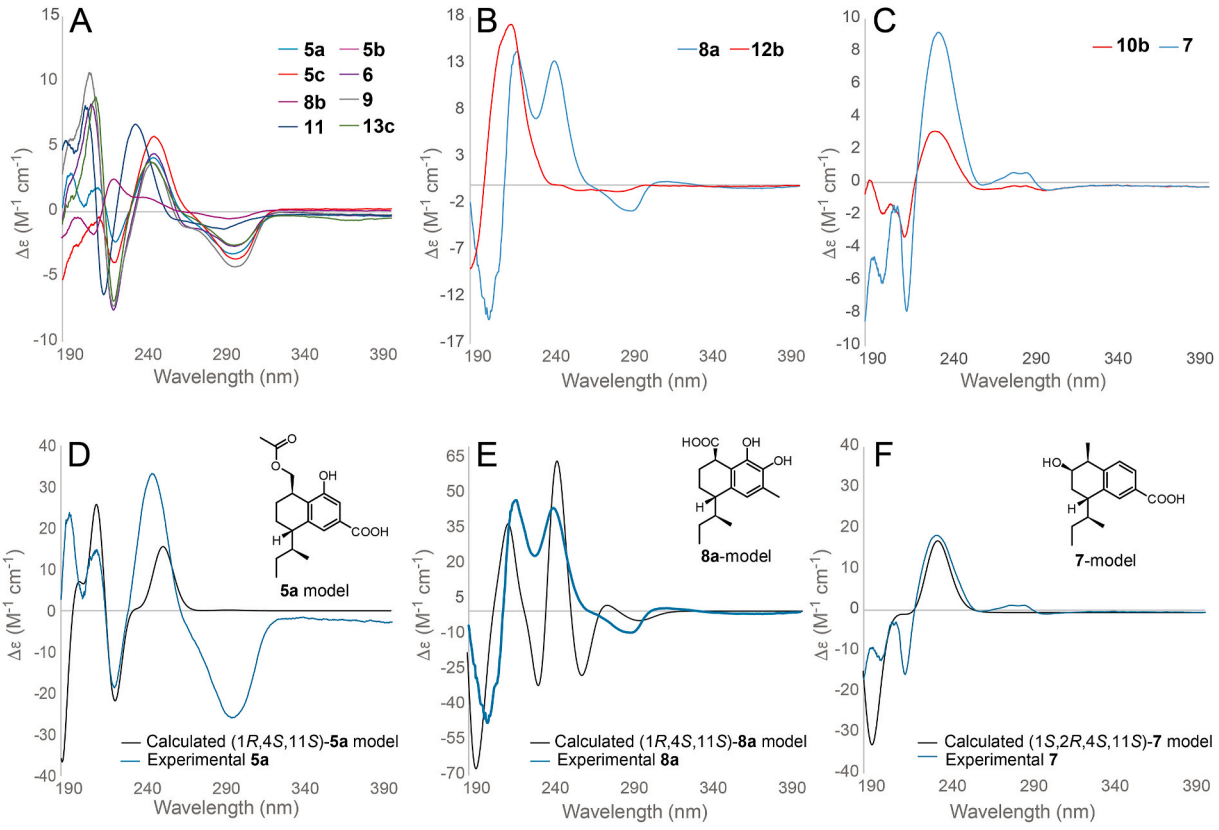

Fig. 4. Experimental and calculated electronic circular dichroism spectra of serrulatane-type diterpenoids. **A**. Experimental ECD of compounds in group A (**5a**, **5b**, **5c**, **6**, **8b**, **9**, **11** and **13c**). **B**. Experimental ECD of compounds in group B (**8a** and **12b**). **C**. Experimental ECD of compounds in group B (**7** and **10b**). **D**. Calculated ECD of (1*R*,4*S*,11*S*)-**5a** model compared to the experimental ECD of **5a**. **E**. Calculated ECD of (1*R*,4*S*,11*S*)-**8a** model compared to the experimental ECD of **8a**. **F**. Calculated ECD of (1*S*,2*R*,4*S*,11*S*)-**7** model compared to the experimental ECD of **7a**.

Table 1
^{1}H NMR (600 MHz) and ^{13}C NMR (150 MHz) spectroscopic data of **5a**, **5c**, **7**, and **8a** (δ in ppm).

No.	5a[a]		5c[a]		7[b]		8a[a]	
	δ_C[c]	δ_H (nH, m, *J* (Hz))	δ_C[c], type	δ_H (nH, m, *J* (Hz))	δ_C[c], type	δ_H (nH, m, *J* (Hz))	δ_C[c], type	δ_H (nH, m, *J* (Hz))
1	33.1	3.40 (1H, m)	33.2	3.39 (1H, m)	38.4	2.99 (1H, qd, $J_{H1,H20} = 7.2$, $J_{H1,H2} = 3.4$)	44.1	3.74 (1H, br t, $J_{H1,H2\alpha} \approx J_{H1,H2\beta} = 6.1$)
2	22.4	1.85 (2H, m, overlap)	22.5	1.83 (2H, m, overlap)	69.9	4.20 (1H, dt, $J_{H2,H3\beta} = 6.6$, $J_{H1,H2} \approx J_{H2,H3\alpha} = 3.4$)	25.5	α: 2.01 (1H, m, overlap) β: 1.93 (1H, m, overlap)
3	20.2	α: 1.86 (1H, m, overlap) β: 1.77 (1H, m)	20.1	α: 1.84 (1H, m, overlap) β: 1.77 (1H, m)	29.6	α: 1.79 (1H, m, overlap)β: 2.08 (1H, ddd, $J_{H3\alpha,\ H3\beta} = 13.9$, $J_{H3\beta,H4} = 7.7$, $J_{H2,H3\beta} = 6.6$)	22.5	α: 1.59 (1H, m overlap) β: 1.91 (1H, m, overlap)
4	43.4	2.67 (1H, m)	43.6	2.67 (1H, m)	40.2	3.11 (1H, td, $J_{H4,\ H3\alpha} \approx J_{H4,H3\beta} = 7.7$, $J_{H4,H11} = 4.4$)	43.1	2.57 (br q, $J_{H2\alpha,\ H4} \approx J_{H2\beta,H4} \approx J_{H4,H11} = 5.2$)
5	122.6	7.37 (1H, br d, $J_{H5,H7} = 1.1$)	122.8	7.35 (1H, br d, $J_{H5,H7} = 1.3$)	129.6	7.99 (1H, br d, $J_{H5,H7} = 1.7$)	121.9	6.51 (1H, s)
6	127.9	–	127.6	–	126.5	–	124.2	–
7	113.6	7.22 (1H, br d, $J_{H5,H7} = 1.1$)	113.7	7.19 (1H, br d, $J_{H5,H7} = 1.3$)	127.5	7.87 (1H, dd, $J_{H7,H8} = 8.1$, $J_{H5,H7} = 1.7$)	141.7	–
8	155.8	–	155.8	–	127.9	7.32 (1H, dd, $J_{H7,H8} = 8.1$, $J_{H1,H8} \approx 0.6$)	144.7	–
9	Nd	–	127.6	–	145.9	–	132.7	–
10	Nd	–	142.5	–	139.1	–	122.0	–
11	39.7	1.96 (1H, m)	39.9	1.97 (1H, m)	37.5	2.19 (1H, m)	37.6	1.97 (1H, m, overlap)
12	30.4	A: 1.18 (1H, m) B: 1.27 (1H, m overlap)	30.6	A: 1.01 (1H, m) B: 1.36 (1H, m)	31.4	1.06 (2H, m, overlap)	33.5	A: 1.02 (1H, overlap) B: 1.23 (1H, m)
13	34.2	A: 1.33 (1H, m, overlap) B: 1.56 (1H, dddd, $J_{H13A,H13B} = 15.5$, $J_{H13B,H12B} = 13.5$, $J_{H13B,H14} = 7.4$, $J_{H13B,H12A} = 4.9$)	34.3	A: 1.35 (1H, m, overlap) B: 1.61 (1H, m, overlap)	26.1	A: 1.80 (1H, m, overlap) B: 1.97 (1H, br dq, $J_{H13A,H13B} \approx 14$, $J_{H13B,H14} \approx J_{H12,H13B} \approx 7$)	26.9	A: 1.85 (1H, br dq,$J_{H13A,\ H13B} \approx 15$, $J_{H12A,\ H13A} \approx J_{H12B,H13A} \approx J_{H13A,H14} \approx 7$) B: 1.97 (1H, m, overlap)
14	76.6	3.87 (1H, br dd, $J_{H13B,H14} = 7.4$, $J_{H13A,H14} = 5.7$)	77.2	3.86 (1H, t, $J_{H13A,H14} \approx J_{H13B,\ H14} = 6.7$)	124.4	4.92 (1H, br t sep, $J_{H13A,H14} \approx J_{H13B,H14} \approx 7$, $J_{H14,\ H16} \approx J_{H14,H17} = 1.2$)	125.5	5.01 (1H, br t sep, $J_{H13A,H14} \approx J_{H13B,H14} \approx 7$, $J_{H14,H16} \approx J_{H14,H17} = 1.5$)
15	148.8	–	148.7	–	131.4	–	131.7	–
16	110.8	A: 4.72 (1H, solvent overlap) B: 4.83 (solvent overlap)	111.4	A: 4.72 (solvent overlap) B: 4.77 (solvent overlap)	25.5	1.63 (3H, br s)	25.6	1.65 (3H, s)
17	17.5	1.61 (3H, br s)	17.4	1.63 (3H, s)	17.6	1.51 (3H, s)	17.6	1.55 (3H, s)
18	19.3	0.99 (3H, d, $J_{H11,\ H18} = 6.9$)	19.1	0.99 (3H, d, $J_{H11,H18} = 6.8$)	17.8	1.04 (3H, d, $J_{H11,H18} = 6.9$)	18.7	0.98 (3H, d, $J_{H11,H18} = 6.9$)
19	173.6	–	175.6	–	169.5	–	16.0	2.17 (3H, s)
20	66.3	A: 4.04 (1H, t, $J_{H20A,\ H20B} \approx J_{H1,H20A} = 10.3$) B: 4.24 (1H, dd, $J_{H20A,\ H20B} = 10.3$, $J_{H1,H20A} = 3.7$)	66.0	A: 4.03 (1H, t, $J_{H1,H20A} \approx J_{H20A,H20B} = 10.4$) B: 4.24 (1H, dd, $J_{H20A,H20B} = 10.4$, $J_{H1,H20A} = 3.8$)	16.6	1.38 (3H, d, $J_{H1,H20} = 7.2$)	180.5	–
	172.9	–	173.3	–	–	–	–	–
	20.9	2.04 (3H, s)	20.6	2.04 (3H, s)	–	–	–	–

[a] Spectral data acquired in methanol-d_4.
[b] Spectral data acquired in chloroform-*d*.
[c] ^{13}C NMR shifts and assignments were based on 2D HSQC and HMBC.

Table 2
^{1}H NMR (600 MHz) and ^{13}C NMR (150 MHz) spectroscopic data of **8b**, **10b**, and **13c** (δ in ppm).

No.	8b[a]		10b[b]		13c[b]	
	δ_C[c], type	δ_H (nH, m, *J* (Hz))	δ_C[c], type	δ_H (nH, m, *J* (Hz))	δ_C[c], type	δ_H (nH, m, *J* (Hz))
1	42.5	3.79 (1H, t, $J_{H1,H2\alpha} \approx J_{H1,H2\beta} = 7.1$)	36.6	3.15 (1H, qd, $J_{H1,H20} = 7.1$, $J_{H1,H2} = 4.0$)	32.5	3.29 (1H, dq, $J_{H1,H20A} = 9.8$, $J_{H1,H2} = {}_{H1,H20B} \approx 2.2$)
2	26.5	α: 2.2 (1H, m) β: 1.79 (1H, dddd, $J_{H2\alpha,H2\beta} = 13.9$, $J_{H2\beta,H3\alpha} = 9.3$, $J_{H1,H2\beta} = 7.1$, $J_{H2\beta,H3\beta} = 3.2$)	72.2	5.31 (1H, ddd, $J_{H2,H3\beta} = 7.3$, $J_{H1,H2} = 4.0$, $J_{H2,H3\alpha} = 2.9$)	21.4	1.87 (2H, m, overlap)
3	22.5	α: 1.61 (1H, m) β: 1.89 (1H, m)	25.9	α: 1.79 (1H, m) β: 2.13 (1H, dt, $J_{H3\alpha,\ H3\beta} = 14.3$, $J_{H2,H3\beta} \approx J_{H3\beta,H4} = 7.3$)	19.1	A: 1.82 (1H, m, overlap) B: 1.88 (1H, m, overlap)
4	44.4	2.75 (1H, br td, $J_{H4,H3\alpha} = J_{H4,H3\beta} = 7.3$, $J_{H4,H11} = 4.6$)	40.8	3.02 (td, $J_{H3\alpha,H4} \approx J_{H3\beta,H4} = 7.3$, $J_{H4,H11} = 4.5$)	42.2	2.69 (1H,m)
5	121.7	7.48 (1H, br s)	129.7	7.98 (1H, d br, $J_{H5,H7} = 1.5$)	123.2	7.47 (1H, d, $J_{H5,H7} = 1.6$)
6	127.6	–	126.6	–	127.5	–
7	113.3	7.22 (1H, d, $J_{H5,H7} = 1.2$)	127.5	7.87 (1H, dd, $J_{H7,H8} = 8.2$, $J_{H5,H7} = 1.5$)	114.9	7.44 (1H, d, $J_{H5,H7} = 1.6$)
8	156.4	–	127.9	7.29 (1H, d, $J_{H7,H8} = 8.2$)	155.2	–
9	127.5	–	146.1	–	127.6	–
10	141.5	–	138.9	–	142.2	–
11	37.1	2.13 (1H, m)	37.1	2.19 (1H, m)	38.2	1.86 (1H, m, overlap)
12	33.5	A: 1.05 (1H, m) B: 1.17 (1H, m)	31.5	1.09 (2H, m)	33.7	A: 1.12 (1H, dtd, $J_{H12A,H12B} = 13.4$, 9.6, 5.1) B: 1.27 (1H, m)
13	27.2	A: 1.87 (1H, m) B: 1.98 (1H, overlap)	26.2	A: 1.82 (1H, m, overlap) B: 1.97 (1H, m, overlap)	26.1	A: 1.99 (1H, m) B: 1.80 (1H, m, overlap)
14	125.6	4.99 (solvent overlap)	124.2	4.93 (1H, br t sep, $J_{H13,H14} = 7.8$, $J_{H14,\ H16} \approx J_{H14,\ H17} = 1.4$)	124.5	4.95 (br t sep, $J_{H13,H14} = 8.5$, $J_{H14,H16} = J_{H14,H17} = 1.4$)
15	131.9	–	131.6	–	131.6	–
16	25.8	1.64 (3H, br d, $J_{H14,H16} = 1.0$)	25.6	1.63 (3H, br s)	25.7	1.64 (3H, s)
17	17.6	1.54 (3H, br d, $J_{H14,H16} = 1.0$)	17.6	1.52 (3H, br s)	17.5	1.54 (3H, s)
18	18.6	1.04 (3H, d, $J_{H11,H18} = 6.9$)	18.1	1.03 (3H, d, $J_{H11,H18} = 6.8$)	18.75	0.96 (3H, d, $J_{H11,H18} = 6.9$)
19	172.2	–	169.2	–	168.8	-
20	178.2	–	16.9	1.29 (3H, d, $J_{H1,H20} = 7.2$)	66.5	A: 3.88 (1H, dd, $J_{H20A,H20B} = 11.5$, $J_{H1,H20A} = 9.8$) B: 4.35 (1H, dd, $J_{H20A,H20B} = 11.5$, $J_{H1,H20B} = 2.2$)
1'	52.3	3.65 (3H, s)	170.7	–	169.9	–
2'	–	–	21.2	2.01 (3H, s)	128	-
3'	–	–	–	–	139.2	6.97 (1H, qq, $J_{H3',H4'} = 7.0$, $J_{H3',H5'} = 1.2$)
4'	–	–	–	–	14.4	1.83 (3H, dq, $J_{H3',H4'} = 7.0$, $J_{H4',H5'} = 1.2$)
5'	–	–	–	–	11.8	1.87 (3H, br t, $J_{H3',H5'} = J_{H4',H5'} = 1.2$)

[a] Spectral data acquired in methanol-d_4.
[b] Spectral data acquired in chloroform-*d*.
[c] ^{13}C NMR shifts and assignments were based on 2D HSQC and HMBC.

in **5c** showed a ROE correlation with H-18, whereas this correlation was not seen for **5a**. Furthermore, a weak ROE correlation between H-14 and H-11 in **5a** suggested the stereochemistry at C-14 to be opposite in the two compounds **5a** and **5c**. However, free rotation at C-11 makes it difficult to determine the stereochemistry, but it is assumed, that compounds **5a** and **5c** are epimers at C-14. Based on biosynthetic arguments, compounds **5a** and **5c** are tentatively assigned the 1*R*,4*S*,11*S* configuration as shown in Fig. 2. To validate the assignment of the stereochemistry at C-1, C-4, and C-11 for **5a** and **5c**, ECD calculation was conducted for the (1*R*,4*S*,11*S*)-**5a model** shown in Fig. 4D. Conformational search for the 3D structure of this model compound resulted in 102 possible conformers, among which 12 dominant ones were used for calculation of ECD spectra (Supplementary data Tables S9 and S10). The experimental and calculated ECD spectra showed high similarities to each other, i.e., two positive Cotton effects were observed around 210 and 250 nm in both spectra. However, the strong negative Cotton effect at around 300 nm in the experimental ECD spectrum was not present in the calculated spectrum, which may be due to the lack of the enol moiety at C-14 to C-16 in the truncated model structure. Compounds **5a** and **5c** were nonetheless identified as C-14-epimers of (1*R*,4*S*,11*S*)-20-acetoxy-8,14-dihydroxyserrulat-15-en-19-oic acid. Thus, compounds **5a** and **5c** were identified as the previously unreported (1*R*,4*S*,11*S*,14*R**)-20-acetoxy-8,14-dihydroxyserrulat-15(16)-en-19-oic acid and (1*R*,4*S*,11*S*,14*S**)-20-acetoxy-8,14-dihydroxyserrulat-15(16)-en-19-oic acid, for which the names eremoglabrane A and eremoglabrane B, respectively, are suggested. ^{1}H and ^{13}C NMR data are provided in Table 1, selected 2D NMR correlations are shown in Fig. 3, ^{1}H and ^{13}C NMR data and all correlations from 2D NMR experiments are provided in Supplementary data Table S2 for **5a** and S3 for **5c**, and ^{1}H NMR, COSY, HSQC, HMBC and ROESY spectra are provided in Supplementary data Figs. S1–S5 for **5a** and S6-S10 for **5c**.

The constituent collected as peak **8a** showed an $[M+H]^+$ ion at *m/z* 333.2066 (calcd. 333.2060, ΔM −1.7), suggesting a molecular formula of $C_{20}H_{28}O_4$, which corresponds to a hydrogen deficiency index of 7. The 1D and 2D NMR spectra indicated that this compound exhibited the same serrulatane core structure as the other compounds isolated in this work, but with altered substitution patterns of the aromatic ring and at C-1. The singlet aromatic proton H-5 (δ_H 6.51) suggested substitutions at aromatic C-6, C-7, and C-8, and a singlet methyl resonance (δ_H 2.17, H_3-19) with HMBC correlations to C-5, C-6, and C-7 confirmed a 6-methylation of the aromatic ring. The molecular formula and the chemical shift of C-7 and C-8 (δ_C 141.7 and δ_C 144.7, respectively) confirmed the 7,8-dihydroxylation of the aromatic ring. An HMBC correlation from H-1 to the carbonylic signal (δ_C 180.5, C-20) confirmed the carboxylic acid

positioned at C-1. The 2D ROESY spectrum furthermore showed correlations between α-oriented H-1, H-2α, and H-3α, and between β-oriented H-4, H-3β and H-2β, whereas no correlation was observed between H-1 and H-4, indicating that these are on opposite sides of the plane, as also observed for all other compounds identified in this work, supporting a 1*R*,4*S* configuration (Fig. 3). Based on biosynthetic considerations as stated above, **8a** was tentatively assigned the 1*R*,4*S*,11*S* configuration. Similar to **7** and **5a**, ECD calculation was used to confirm the absolute configuration of **8a**. Conformational search for the 3D structure of (1*R*,4*S*,11*S*)-**8a model** (Fig. 4E) led to 33 possible conformers, among which 9 dominant ones were used for calculation of ECD spectra (Supplementary data Tables S13 and S14). As shown in Fig. 4E, both the calculated and experimental ECD spectra were characterized by two positive Cotton effects around 220 and 245 nm, and two negative bands near 230 and 290 nm, even though the relative intensities were not perfectly reproduced, likely due to the truncated side chain of the model structure. Thus, compound **8a** was identified as the previously unreported (1*R*,4*S*,11*S*)-7,8-dihydroxyserrulat-14-en-20-oic acid, for which the name eremoglabrane D is suggested. ^{1}H and ^{13}C NMR data are provided in Table 1, selected 2D NMR correlations are shown in Fig. 3, ^{1}H and ^{13}C NMR data and all correlations from 2D NMR experiments are provided in Supplementary data Table S5, and ^{1}H NMR, COSY, HSQC, HMBC and ROESY spectra are provided in Supplementary data Figs. S16–S20.

The constituent collected as peak **8b** showed an $[M+H]^+$ ion at *m/z* 361.2004 (calcd. 361.2010, ΔM +1.5), suggesting a molecular formula of $C_{21}H_{28}O_5$, which corresponds to a hydrogen deficiency index of 8. As for other compounds isolated in this work, 1D and 2D NMR spectra revealed a serrulatane core structure. The 1D ^{1}H-NMR data showed two meta-coupled aromatic protons at δ_H 7.22 (br d, $J_{H5,H7}$ = 1.2 Hz, H-7) and δ_H 7.48 (br s, H-5), and HMBC correlations from H-5 and H-7 to a carbonylic signal (δ_C 172.2, C-19), confirmed the carboxylic acid attached to C-6. An HMBC correlation from H-7 to an oxygenated, quaternary carbon (δ_C 156.4, C-8) revealed hydroxylation at C-8. These data are in agreement with the previously reported NMR data of the aromatic ring of the closely related serrulatane **9** (Ndi et al., 2007). The methoxy singlet for H-1' (δ_H 3.65, δ_C 52.3) as well as H-1 (δ 3.79 t, $J_{H1,H2a} = J_{H1,H2b}$ = 7.1) showed HMBC correlations to a carbonyl ester (δ_C 178.2, C-20), which confirmed the methoxycarbonyl attached to C-1. The 2D ROESY spectrum showed correlations between the α-oriented H-1, H-2α, and H-3α, and between β-oriented H-4, H-3β and H-2β (Fig. 3). Based on biosynthetic considerations, compound **8b** was tentatively assigned the 1*R*,4*S*,11*S* configuration. The experimental ECD spectrum of **8b** (Fig. 4A), has the same overall curvature as the other spectra in class A, albeit with a small blue shift as it is the only compound with carboxylic acid at C-1, and **8b** displays a negative Cotton effect around 220 nm, and a positive Cotton effect around 230 nm (in addition to a small positive Cotton effect around 245 nm. Thus, based on the experimental ECD spectrum and biosynthetic considerations, *vide supra*, **8b** was identified as the previously unreported (1*R*,4*S*,11*S*)-20-methoxycarbonyl-8-hydroxyserrulat-14-en-19-oic acid, for which the name eremoglabrane E is suggested. ^{1}H and ^{13}C NMR data are provided in Table 2, selected 2D NMR correlations are shown in Fig. 3, ^{1}H and ^{13}C NMR data and all correlations from 2D NMR experiments are provided in Supplementary data Table S6, and ^{1}H NMR, COSY, HSQC, HMBC and ROESY spectra are provided in Supplementary data Figs. S21–S25.

The constituent collected as peak **10b** showed an $[M+H]^+$ ion at *m/z* 359.2225 (calcd. 359.2230, ΔM −2.3), suggesting a molecular formula of $C_{22}H_{30}O_4$, corresponding to a hydrogen deficiency index of 8. Compound **10b** showed a ^{1}H-NMR spectrum very similar to that of **7**, with identical resonances for most of the hydrogens. However, a change in chemical shift from δ_H 4.20 to δ_H 5.31 for H-2 and an additional methyl resonance at δ_H 2.01 ppm (H_3-2′) with an HMBC correlation to a carbonylic signal (δ_C 170.7 ppm, C-1′) was observed, confirming the acetoxylation of C-2. This change correlated with the molecular formula observed for this compound. The 2D ROESY spectrum accordingly also showed ROE correlations very similar to that of **7**, indicating the same relative stereochemistry for compound **10b**, and the absolute configuration of **10b** was tentatively assigned the 1*S*,2*R*,4*S*,11*S* configuration. The experimental ECD spectrum for **10b** (Fig. 4C) showed a negative Cotton effect at 215 nm and a positive cotton effect at 235 nm, which is very similar to that of **7**, further supporting that the absolute configuration of **10b** is the same as that for **7**. Thus, compound **10b** was identified as the previously unreported (1*S*,2*R*,4*S*,11*S*)-2-acetoxyserrulat-14-en-19-oic acid, for which the name eremoglabrane F is suggested. ^{1}H and ^{13}C NMR data are provided in Table 2, selected 2D NMR correlations are shown in Fig. 3, ^{1}H and ^{13}C NMR data and all correlations from 2D NMR experiments are provided in Supplementary data Table S7, and ^{1}H NMR, COSY, HSQC, HMBC and ROESY spectra are provided in Supplementary data Figs. S26–S30.

The constituent collected as peak **13c** showed an $[M+H]^+$ ion at *m/z* 415.2464 (calcd. 415.2479, ΔM +3.6), suggesting a molecular formula of $C_{25}H_{34}O_5$, which corresponds to a hydrogen deficiency index of 9. The 1D and 2D NMR data suggested an 8-hydroxyserrulat-14-ene-19-oic acid structure, as described previously for compound **8b**. Comparing the NMR data of compound **13c** with that of **8b** and **9** revealed a different substitution at C-1. Thus, an olefinic proton at δ_H 6.97 (qq, $J_{H3',H4'}$ = 7.0, $J_{H3',H5'}$ = 1.2, H-3′) with COSY correlations to H_3-4' (δ_H 1.83, dq, $J_{H3',H4'}$ = 7.0, $J_{H4',H5'}$ = 1.2) and H_3-5' (δ_H 1.87, br t $J_{H3',H5'} = J_{H4',H5'}$ = 1.2) and an HMBC correlation to a carbonylic signal (δ_C 169.9, C-1′) revealed the presence of an angelic acid. Furthermore, HMBC correlations from H-5′ to C-1′ and from H-20 to C-1′ confirmed the angelic acid moiety being attached to C-20. The 2D ROESY spectrum showed correlations consistent with the other serrulatanes isolated in this work, with H-4 correlating with H-5, H-11, and H-18, and no correlations between H-1 and H-4, supporting that the configuration is the same throughout all serrulatanes isolated here. The experimental ECD spectrum of **13c** showed positive Cotton effects around 210 and 250 nm and negative Cotton effects around 225 and 300 nm (Fig. 4A), as do the remaining spectra in class A, and in agreement with that of the calculated spectrum of **5a** (except for the negative band at 300 nm as discussed above). Compound **13c** was therefore identified as the previously unreported (1*R*,4*S*,11*S*)-20-angeloyloxy-8-hydroxyserrulat-14-en-19-oic acid, for which the name eremoglabrane G is suggested. ^{1}H and ^{13}C NMR data are provided in Table 2, selected 2D NMR correlations are shown in Fig. 3, ^{1}H and ^{13}C NMR data and all correlations from 2D NMR experiments are provided in Supplementary data Table S8, and ^{1}H NMR, COSY, HSQC, HMBC and ROESY spectra are provided in Supplementary data Figs. S31–S35.

Eremophila is the major genus in the tribe Myoporeae. Recent extensive phylogenetic studies based on nuclear ribosomal DNA sequencing divided the Myoporeae into eight clades labelled A to H (Gericke et al., 2021). Clade H is divided into 14 subclades, H1 to H14, of which the H14 subclade is characterized by species having resinous leaves and a unique chemical signature indicating a large unknown chemical space of serrulatane chemistry with substructural motif blooms (Gericke et al., 2021). *E. glabra*, the focus species of our current study, belongs to the H14 subclade and our isolation of twelve serrulatane-type diterpenoids of which seven were previously unknown natural products serves to start filling this unknown chemical space with known

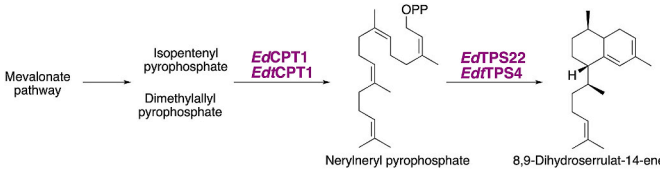

Fig. 5. Initial steps in serrulatane-type diterpenoid biosynthesis in *Eremophila*. Ed: *E. drummundii*, Edt: *E. denticulata* subsp. *trisculata*. CPT: *cis*-prenyl transferase. TPS: class I terpene synthase.

structures.

The initial steps in the biosynthesis of serrulatane-type diterpenoids have recently been studied in *E. drummondii* and *E. denticulate* subsp. *trisulcata* (Gericke et al., 2020). These two species are also positioned within the H14 subclade indicating that the same biosynthetic intermediates would be involved in *E. glabra*. From both species, a *cis*-prenyltransferase was identified catalyzing the formation of nerylneryl diphosphate from the C5 isoprenoids IPP and DMAPP (Fig. 5). The nerylneryl diphosphate is then converted to the serrulatane backbone by the activity of a class I terpene synthase to produce 8,9-dihydroserrulat-14-ene, which is rapidly aromatized to serrulat-14-ene in a non-enzymatic reaction (Gericke et al., 2020). The final decoration of the serrulatane backbone is expected to involve the action of cytochrome P450s as well as acetyl-, angelate-, and methyl transferases. Thus, multiple P450 oxygenations of the C1- and C19-methyl groups are envisioned to give rise to the introduction of carboxyl group in **5a, 5b, 5c**, **6**, **7**, **8b**, **9**, **10b**, **11**, and **13c** (Hansen et al., 2021), whereas single oxygenation reactions are observed at C-2, C-7, C-8, C-14, and C-20 dependent on the compound, likewise envisioned to be P450-catalysed (Hansen et al., 2021). Esterification with acetic acid and angelic acid, observed at C-2 and/or C-20 in **5a**/**5c**, **9**, **10b**, **11**, and **13c**, involves acetyl transferases and a putative angelic acid transferase (Luo et al., 2016; Callari et al., 2018; Wang et al., 2021). Additional modification of **8b** involves methyl ether formation catalysed by a methyltransferase.

The biosynthesis of *Eremophila* diterpenoids, *i.e.*, serrulatane diterpenoids, from the cisoid precursor nerylneryl diphosphate rather than from the transoid precursor geranylgeranyl diphosphate is manifested in the unique diterpenoid structures discovered in the present study.

2.3. α-Glucosidase and PTP1B inhibitory activity of the isolated serrulatane-type diterpenoids

Compounds **4**, **5a**, **5b**, **5c**, **8a**, **8b**, **10b**, **12b**, and **13c** were evaluated for α-glucosidase inhibitory activity at 200 or 100 μM, and compounds **2**, **4**, **5a**, **5b**, **5c**, **6**, **7**, **8a**, **8b**, **9**, **10b**, **11**, **12b**, and **13c** were evaluated for PTP1B inhibitory activity at the same concentrations (Table 3). Dilution series of **8a**, **12b**, and **13c** were tested for PTP1B inhibitory activity and a dilution series of **8a** was tested for α-glucosidase inhibitory activity (Supplementary data Figs. S37 and S38). Compounds **8a**, **12b**, and **13c** showed IC_{50} values of 64 ± 6 μM, 64 ± 15 μM, and 104 ± 26 μM, respectively, for PTP1B, and **8a** showed an IC_{50} of 147 ± 25 μM for α-glucosidase. The PTP1B positive control RK-682 showed an IC_{50} value of 12.1 ± 1.1 μM, which means that compounds **8a**, **12b** and **13c** are weak inhibitors of PTP1B relative to the reference compound. Compound **8a** showed an IC_{50} value against α-glucosidase that was approximately 10-fold lower than that of the positive control acarbose (1253.5 ± 118.2 μM), making it a better inhibitor than acarbose. Acarbose is however not a strong inhibitor, which further accentuates the need for identification of improved α-glucosidase inhibitors with reduced side-effects. Of the here isolated serrulatane-type diterpenoids, only a few showed inhibitory activity against α-glucosidase and PTP1B. Structurally, **8a** and **12b** are the only two compounds carrying a double hydroxylated aromatic ring and no C-19-carboxyl group. These features may contribute to their PTP1B activity.

Table 3
PTP1B and α-glucosidase inhibitory activities of the isolated compounds at 200 or 100 μM.

Compound	Concentration (μM)	PTP1B inhibition (%)	α-glucosidase inhibition (%)
2	200	38.9 ± 8.0	–
5a	200	26.4 ± 4.6	77.7 ± 2.6
5b	200	3.0 ± 9.7	−40.4 ± 3.7
5c	100	26.1 ± 2.3	48.6 ± 3.9
4	200	22.0 ± 11.0	42.9 ± 6.7
6	200	36.1 ± 4.5	–
7	200	15.9 ± 8.1	–
8a	200	94.5 ± 2.4	73.2 ± 6.5
8b	200	31.5 ± 1.6	31.5 ± 1.6
9	200	50.3 ± 3.3	–
10b	200	28.1 ± 3.7	−43.3 ± 7.7
11	200	64.6 ± 3.9	–
12b	200	84.2 ± 3.5	39.3 ± 7.7
13c	100	88.5 ± 5.2	40.0 ± 7.4

3. Conclusions

In conclusion, the use of high-resolution α-glucosidase and PTP1B inhibition profiling of the crude leaf resin extract of *E. glabra* in combination with HPLC-PDA-HRMS, semi-preparative-scale HPLC, and NMR spectroscopy, led to the identification of serrulatane-type diterpenoids with moderate α-glucosidase and/or PTP1B inhibitory activity. However, seven previously unreported serrulatane diterpenoids were isolated and identified together with four previously reported flavonoids and five previously reported serrulatane diterpenoids. Two of the serrulatane diterpenoids showed weak PTP1B inhibitory activity and one exhibited dual α-glucosidase and PTP1B inhibitory activity. This study thus substantiates that species in *Eremophila* are a rich source of previously unreported serrulatane diterpenoids and that *Eremophila* is a valuable genus in the search for antidiabetic drug leads.

Eremophila spp. are culturally important plants for many of Australia's First Peoples, the Aboriginal peoples. If you use the information here provided to make commercial products, we urge you to strongly consider benefit sharing with the Aboriginal communities or groups in the areas where these species grow. We acknowledge that this work took place on the lands of Aboriginal peoples who are the custodians of this land and acknowledge and pay our respects to their Elders, past and present.

4. Experimental

4.1. Chemicals

Calcium acetate and formic acid were purchased from Merck (Darmstadt, Germany). Recombinant human protein tyrosine phosphatase 1B (PTP1B) (BML-SE332-0050, EC 3.1.3.48) was purchased from Enzo Life Sciences. (NY, USA). Methanol-d_4, DMSO-d_6, and chloroform-*d* were purchased from Euriso-top (Gif-Sur-Yvette, France). HPLC-grade acetonitrile and methanol were purchased from VWR international (Fontenay-Sous-Bois). Water was purified by deionization and 0.22 μM membrane filtration (Millipore, Billerica, MA, USA). All other chemicals were purchased from Sigma-Aldrich (St. Louis, MO, USA).

4.2. Plant material and extraction

Leaves of *Eremophila glabra* (R.Br.) Ostenf. (Scrophulariaceae) were collected from several individual plants in August 2017 at Lake Kerrylyn, North of Mt Methwin, Western Australia, Australia (25 02 42.3 S; 120 44 30.5 E) and identified by Dr Bevan Buirchell. The material was stored at −20 °C until extraction. A voucher specimen has been deposited at the University of Melbourne Herbarium, Melbourne, Victoria, Australia (accession number MELUD127890a). To extract the leaf resins, the leaf material (48.0 g) was submerged in 200 mL of acetonitrile and shaken for 10 min (Ratek, Knox City, VIC, Australia). The extract was then filtered using a glass funnel, and the filtrate was dried *in vacuo* at 45 °C using a IKA RV10 rotary evaporator (IKA Werke, Staufen, Germany). The dried matter (2.41 g) was re-dissolved into a small volume of methanol, transferred to amber vials, dried under a stream of nitrogen gas, and then stored at −20 °C until use.

4.3. α-Glucosidase and PTP1B assays

The α-glucosidase inhibition assay was performed at 28 °C using 96

well microplates. A phosphate buffer consisting of 0.066 M Na_2HPO_4 and 0.034 M $NaH_2PO_4 \cdot H_2O$ with 0.02% NaN_3 was adjusted to pH 7.5 with NaOH. All analytes were dissolved in buffer containing 10% DMSO, and 5 μl of a 2 U/mL α-glucosidase were added to each well together with 75 μL phosphate buffer. The microplates were incubated for 10 min at 28 °C, followed by the addition of 20 μL substrate solution (10 mM *p*-NPG) to a final volume of 200 μL pr. well. The absorbance at 405 nm was measured every 30 s for 35 min using a Thermo Fisher Scientific Multiscan FC microplate reader (Thermo Scientific, Waltham, MA, USA) coupled to SkanIt ver. 2.5.1 software. The percentage of α-glucosidase inhibition was calculated using the following equation:

$$\text{Percentage inhibition} = \left(1 - \frac{\text{Slope}_{\text{sample}}}{\text{Slope}_{\text{blank}}}\right) \cdot 100\%$$

The PTP1B inhibition assay was performed at 25 °C using 96 well microplates. A buffer consisting of 50 mM Tris, 50 mM bis-tris and 100 mM NaCl was adjusted to pH 7.0 with phosphoric acid. All analytes were dissolved in 18 μL DMSO and 52 μL 3.46 mM EDTA solution, followed by the addition of 60 μL substrate solution (1.5 mM *p*-NPP and 6 mM DTT) to each well. The plates were incubated for 10 min at 25 °C, and 50 μL 0.001 μg/μL PTP1B solution were added to each well. The absorbance was measured at 405 nm every 30 s for 10 min, and the percentage PTP1B inhibition was calculated as described for α-glucosidase.

4.4. High-resolution inhibition profiling of crude extract

Analytical-scale HPLC separation and micro-fractionation of the crude *E. glabra* extract was performed using an Agilent 1200 system (Santa Clara, CA, USA) consisting of a G1367C high-performance auto sampler, a G1311A quaternary pump, a G1322A degasser, a G1316A thermostatted column compartment, a G1315C photodiode array detector and a G1364C fraction collector, controlled by Agilent ChemStation software ver. B.03.02. The dried crude extract was dissolved in acetonitrile to a concentration of 25 mg/mL for α-glucosidase inhibition profiling and 20 mg/mL for PTP1B inhibition profiling, and 8 μL was injected and separated by a reversed phase Phenomenex Luna C_{18}(2) (150 × 4.6 mm i.d, 3 μm particle size) column (Phenomenex, Torrance, CA, USA) at 40 °C. The flow rate was 0.5 mL/min and solvents A (water/acetonitrile, 95:5, 1% formic acid, v/v/v) and B (water/acetonitrile, 5:95, 0.1% formic acid, v/v/v) were used for gradient elution: 0 min, 10% B; 10 min, 20% B; 45 min, 85% B; 55 min, 100% B; 65 min, 100% B. The 20–60 min eluate was collected into 96-well plates (2 × 176 wells), giving a resolution of 4.4 data points per min. The well contents were evaporated to dryness using a vacuum centrifuge connected to a freeze trap, and α-glucosidase and PTP1B inhibition profiling was performed for each plate using the methods described in 4.3. The inhibition percentages were plotted against respective chromatographic retention times, constructing a high-resolution α-glucosidase and PTP1B inhibition profile (biochromatogram) for the crude extract.

4.5. Isolation of pure compounds

The dried crude extract was dissolved in acetonitrile at a concentration of 20 mg/mL, and separated using a semi-preparative scale Shimadzu system, consisting of a SIL-20A autosampler, a LC-20AD pump, a CTO-10AS column oven, a SPD-20A UV/VIS detector and a FRC-10A fraction collector. The separations were performed on a Phenomenex Luna C_{18}(2) reversed phase column (250 × 10.0 mm i.d., 5 μm particle size, 100 Å pore size, Phenomenex, Torrance, CA USA) with a flow rate of 4 mL/min. Eluent A consisted of water:acetonitrile (95:5, v/v), and eluent B of water:acetonitrile (5:95, v/v), both acidified with 0.1% formic acid. Separations were performed from injections of 100 μL crude extract (20 mg/mL), and peaks were collected manually in 12 fractions, using the elution gradient profile as stated in 4.4. The peaks 5, 7, 8, 10, 12 and 13 were subsequently separated and collected using a Phenomenex Kinetex PFP column (150 × 4.6 mm i.d, 2.6 μm particle size, 100 Å pore size) at 30 °C, using an Agilent 1200 system (as stated in 4.4). Eluent A consisted of water:acetonitrile (95:5, v/v), eluent B of water:acetonitrile (5:95, v/v), eluent C of water-methanol (95:5, v/v), and eluent D of water-methanol (5:95, v/v), all acidified with 0.1% formic acid. The fractions were separated using the following elution gradient profiles: 0 min, 60% D; 5 min, 60% D; 30 min, 70% D, 31 min 100% D; 37 min, 100% D (fraction 4), 0 min, 45% B; 45 min, 65% B; 46 min, 100% B, 52 min, 100% B (fraction 8), 0 min, 30% B; 26 min, 50% B; 27 min, 100% B; 32 min, 100% B (fraction 6), 0 min, 50% B; 20 min, 50% B; , 21 min, 100% B; 29 min, 100% B (fraction 10), 0 min, 52% B; 50 min, 58% B; 51 min, 100% B; 56 min, 100% B (fraction 12), 0 min, 63% B; 40 min, 67% B; 41 min, 100% B; 47 min, 100% B (fraction 13).

4.5.1. Eremoglabrane A [(1R,4S,11S,14R*)-20-acetoxy-8,14-dihydroxyserrulat-15(16)-en-19-oic acid] (**5a**)

Colourless oil; ^{1}H NMR (methanol-d_4, 600 MHz) and ^{13}C NMR (methanol-d_4, 150 MHz) spectroscopic data, Table 1; HRESIMS *m/z* 391.2111 $[M+H]^+$ (calcd. for $C_{22}H_{31}O_6$, 391.2115).

4.5.2. Eremoglabrane B [(1R,4S,11S,14S*)-20-acetoxy-8,14-dihydroxyserrulat-15(16)-en-19-oic acid] (**5c**)

Colourless oil; ^{1}H NMR (methanol-d_4, 600 MHz) and ^{13}C NMR (methanol-d_4, 150 MHz) spectroscopic data, Table 1; HRESIMS *m/z* 391.2105 $[M+H]^+$ (calcd. for $C_{22}H_{31}O_6$, 391.2115).

4.5.3. Eremoglabrane C [(1S,2R,4S,11S)-2-hydroxyserrulat-14-en-19-oic acid] (**7**)

Colourless oil; ^{1}H NMR ($CDCl_3$, 600 MHz) and ^{13}C NMR ($CDCl_3$, 150 MHz) spectroscopic data, Table 1; HRESIMS *m/z* 317.2109 $[M+H]^+$ (calcd. for $C_{20}H_{29}O_3$, 317.2111).

4.5.4. Eremoglabrane D [(1R,4S,11S)-7,8-dihydroxyserrulat-14-en-20-oic acid] (**8a**)

Colourless oil; ^{1}H NMR (methanol-d_4, 600 MHz) and ^{13}C NMR (methanol-d_4, 150 MHz) spectroscopic data, Table 1; HRESIMS *m/z* 333.2066 $[M+H]^+$ (calcd. for $C_{20}H_{29}O_4$, 333.2060).

4.5.5. Eremoglabrane E [(1R,4S,11S)-20-methoxycarbonyl-8-hydroxyserrulat-14-en-19-oic acid] (**8b**)

Colourless oil; ^{1}H NMR (methanol-d_4, 600 MHz) and ^{13}C NMR (methanol-d_4, 150 MHz) spectroscopic data, Table 2; HRESIMS *m/z* 361.2004 $[M+H]^+$ (calcd. for $C_{21}H_{29}O_5$, 361.2010).

4.5.6. Eremoglabrane F [(1S,2R,4S,11S)-2-acetoxyserrulat-14-en-19-oic acid] (**10b**)

Colourless oil; ^{1}H NMR ($CDCl_3$, 600 MHz) and ^{13}C NMR ($CDCl_3$, 150 MHz) spectroscopic data, Table 2; HRESIMS *m/z* 359.2225 $[M+H]^+$ (calcd. for $C_{22}H_{31}O_4$, 359.2230).

4.5.7. Eremoglabrane G [(1R,4S,11S)-20-angeloyloxy-8-hydroxyserrulat-14-en-19-oic acid] (**13c**)

Colourless oil; ^{1}H NMR ($CDCl_3$, 600 MHz) and ^{13}C NMR ($CDCl_3$, 150 MHz) spectroscopic data, Table 2; HRESIMS *m/z* 415.2464 $[M+H]^+$ (calcd. for $C_{25}H_{35}O_5$, 415.2479).

4.6. HPLC-PDA-HRMS analysis

All HPLC-PDA-HRMS analyses were performed using an analytical-scale Agilent 1260 HPLC system (Agilent Technologies, Palo Alto, CA, USA), consisting of a G1329B autosampler, a G1311B quaternary pump with build-in degasser, a G1316A thermostatted column compartment and a G1316A photodiode array detector. Separations were performed at 30 °C on a Phenomenex Luna C_{18}(2) reversed-phase column (150 × 4.6 mm i.d., 3 μm particle size, 100 Å pore size (Phenomenex, Torrance, CA, USA)), with a flow rate of 0.5 mL/min. Eluent A consisted of water:

acetonitrile (95:5, v/v), and eluent B of water:acetonitrile (5:55, v/v), both acidified with 0.1% formic acid. The crude extract was separated using an elution gradient profile as described in 4.4 and pure compounds were eluted with an elution gradient profile from 0 to 100% B in 25 min. The eluate was connected to a T-piece splitter directing 1% of the eluate to a Bruker micrOTOF-Q mass spectrometer equipped with an electrospray ionization (ESI) interface (Bruker Daltonik, Bremen, Germany). Mass spectra were acquired in positive ionization mode, using a drying temperature of 200 °C, a capillary voltage of 4100 V, a nebulizer pressure of 2.0 bar, and a drying gas flow of 7 L/min. Chromatographic separation and mass spectrometry were controlled using Hystar ver. 3.2 software (Bruker Daltonik, Bremen, Germany).

4.7. NMR acquisition and analysis

Purified compounds were dissolved in either DMSO-d_6, methanol-d_4 or chloroform-*d* and transferred to 1.7-mm NMR tubes. All NMR experiments were acquired with a Bruker Avance III 600 MHz NMR spectrometer (^{1}H operating frequency 600.13 MHz) equipped with a Bruker SampleJet autosampler and a 1.7-mm TCI cryoprobe (Bruker Biospin, Karlsruhe, Germany). Acquisitions were recorded with temperature equilibration to 300 K, optimization of lock parameters, gradient shimming and setting of receiver gain, controlled by IconNMR ver. 4.2 (Bruker Biospin, Karlsruhe, Germany). The ^{1}H NMR spectra were acquired with 30-degree pulses and 64k data points, a spectral width of 20 ppm, 1.0 s relaxation decay, and an acquisition time of 2.72 s. NOESY and DQF-COSY 2D data were acquired with a spectral width of 12 ppm and 2k × 512 data points. HSQC spectra were acquired with spectral widths of 12 ppm and 170 ppm for ^{1}H and ^{13}C, respectively, collecting 2k × 512 data points with a relaxation decay of 1.0 s. HMBC spectra were acquired with spectral widths of 12 ppm and 240 ppm for ^{1}H and ^{13}C, respectively, collecting 2k × 512 data points with a relaxation decay of 1.0 s. All NMR data were processed using Topspin (ver. 3.6.0, Bruker Biospin).

4.8. ECD calculation and ECD data acquisition

To reduce the computational cost, the conformational search and DFT calculations of **5a**, **7**, and **8a** were conducted for model structures **5a-**, **7-** and **8a-model** (Fig. 2) for each of them by cutting off the terminal structural unit from C-14 to C-17 of the side chain. Conformational searches were performed with the Molecular Merck force field static (MMFFs) using MacroModel interfaced to Schrödinger Maestro 11.9 (Schrödinger, LLC, USA) (Habgood et al., 2020). The resultant conformers within 5.02 kcal/mol of relative energy were further optimized using Density Functional Theory (DFT) by locating minima on the potential energy surface as provided by the B3LYP functional with the 6-31G (d,p) basis set (Pescitelli and Bruhn, 2016). The effect of acetonitrile solvent was incorporated using the polarizable continuum model in its integral equation formalism (IEF-PCM) (Tomasi et al., 2005). Subsequent DFT calculations were carried out for each optimized conformer accounting for more than 1% of the Boltzmann population using the Gaussian 16 program package (Frisch et al., 2016). Oscillator strengths and rotatory strengths of the first 60 excited states of each conformer were calculated using time-dependent (TD)DFT with the CAM-B3LYP functional and the 6-31G (d,p) basis set, and IEF-PCM for the solvent effects of acetonitrile. The final calculated ECD spectra were obtained after Boltzmann averaging the spectra of all identified conformers. The final calculated ECD spectra were exported using SpecDis software ver. 1.71 (Berlin, Germany) (Bruhn et al., 2017) with a half-bandwidth of 0.20 eV for model structures of **5a** and **7** and 0.25 eV for that of **8a**. Experimental ECD spectra of **5a**, **7** and **8a** were acquired on a JASCO J-1500 CD spectrometer (JASCO, Tokyo, Japan) in acetonitrile in a quartz cuvette (1 cm path length). Each acquisition was performed at 25 °C using the following parameters: wavelength 190–400 nm, scan speed 50 nm/min, digital integration time 4 s, bandwidth 5.0 mm, 5 accumulations.

Funding

HPLC equipment used for high-resolution bioassay profiles was obtained via a grant from The Carlsberg Foundation. The HPLC-HRMS and NMR system used in this work was acquired through a grant from "Apotekerfonden af 1991", The Carlsberg Foundation, and the Danish Agency for Science, Technology, and Innovation via the National Research Infrastructure funds. The Novo Nordisk Foundation is acknowledged for support from the Interdisciplinary Synergy Programme (grant NNF16OC0021616 "Desert-loving therapeutics") to BLM and DS.

Declaration of competing interest

The authors declare that they have no known competing financial interests or personal relationships that could have appeared to influence the work reported in this paper.

Acknowledgments

Arife Önder is acknowledged for technical assistance.

Appendix A. Supplementary data

Supplementary data to this article can be found online at https://doi.org/10.1016/j.phytochem.2021.113072.

References

Algreiby, A.A., Hammer, K.A., Durmic, Z., Vercoe, P., Flematti, G.R., 2018. Antibacterial compounds from the Australian native plant *Eremophila glabra*. Fitoterapia 126, 45–52. https://doi.org/10.1016/j.fitote.2017.11.008.

Atanasov, A.G., Zotchev, S.B., Dirsch, V.M., Supuran, C.T., 2021. Natural products in drug discovery: advances and opportunities. Nat. Rev. Drug Discov. 20, 200–216. https://doi.org/10.1038/s41573-020-00114-z.

Botirov, E.K., Karimov, A.M., 2018. Flavonoids from roots of *Scutellaria intermedia*. Chem. Nat. Compd. 54, 577–578. https://doi.org/10.1007/s10600-018-2412-1.

Brown, A., Buirchell, B.J., 2011. A Field Guide to the Eremophilas of Western Australia. Simon Nevill Publications, York.

Bruhn, T., Schaumlöffel, A., Hemberger, Y., Pecitelli, G., 2017. SpecDis Version 1.71; Berlin, Germany. https://specdis-software.jimdo.com.

Callari, R., Fischer, D., Heider, H., Weber, N., 2018. Biosynthesis of angelyl-CoA in *Saccharomyces cerevisiae*. Microb. Cell Factories 17, 72. https://doi.org/10.1186/s12934-018-0925-8.

Chatterjee, S., Khunti, K., Davies, M.J., 2017. Type 2 diabetes. Lancet 389, 2239–2251. https://doi.org/10.1016/S0140-6736(17)30058-2.

Croft, K.D., Ghisalberti, E.L., Jefferies, P.R., Proudfoot, G.M., 1981. The chemistry of *Eremophila* spp. XVI. New serrulatanes from *Eremophila* spp. Aust. J. Chem. 34, 1951–1957. https://doi.org/10.1071/CH9811951.

Forster, P.G., Ghisalberti, E.L., Jefferies, P.R., Poletti, V.M., Whiteside, N.J., 1986. Serrulatane diterpenes from *Eremophila* spp. Phytochemistry 25, 1377–1383. https://doi.org/10.1016/S0031-9422(00)81293-5.

Frisch, M.J., Trucks, G.W., Schlegel, H.B., Scuseria, G.E., Robb, M.A., Cheeseman, J.R., Scalmani, G., Barone, V., Petersson, G.A., Nakatsuji, H., et al., 2016. Gaussian 16, Revision C.01. Gaussian, Inc., Wallingford CT.

Galic, S., Hauser, C., Kahn, B.B., Haj, F.G., Neel, B.G., Tonks, N.K., Tiganis, T., 2005. Coordinated regulation of insulin signaling by the protein tyrosine phosphatases PTP1B and TCPTP. Mol. Cell Biol. 25, 819–829. https://doi.org/10.1128/MCB.25.2.819-829.2005.

Gericke, O., Hansen, N.L., Pedersen, G.B., Kjaerulff, L., Lou, D., Staerk, D., Møller, B.L., Pateraki, I., Heskes, A.M., 2020. Nerylneryl diphosphate is the precursor of serrulatane, viscidane and cembrane-type diterpenoids in *Eremophila* species. BMC Plant Biol. 20, 91. https://doi.org/10.1186/s12870-020-2293-x.

Gericke, O., Fowler, R.M., Heskes, A.M., Bayly, M.J., Semple, S.J., Ndi, C.P., Staerk, D., Løland, C.J., Murphy, D.J., Buirchell, B.J., Møller, B.L., 2021. Navigating through chemical space and evolutionary time across the Australian continent in plant genus *Eremophila*. Plant J. 108, 555–578. https://doi.org/10.1111/tpj.15448.

Ghisalberti, E.L., 1994. The ethnopharmacology and phytochemistry of *Eremophila* species (Myoporaceae). J. Ethnopharmacol. 44, 1–9. https://doi.org/10.1016/0378-8741(94)90092-2.

Habgood, M.J., James, T., Heifetz, A., 2020. Conformational searching with quantum mechanics. In: Heifetz, A. (Ed.), Quantum Mechanics in Drug Discovery. Springer Science+Business Media, LLC, part of Springer Nature, New York, p. 207. https://doi.org/10.1007/978-1-0716-0282-9_14.

Hansen, C.C., Nelson, D.R., Møller, B.L., Werck-Reichhart, D., 2021. Plant cytochrome P450 plasticity and evolution. Mol. Plant 14, 1244–1265. https://doi.org/10.1016/j.molp.2021.06.028.

Hjortness, M.K., Riccardi, L., Hongdusit, A., Ruppe, A., Zhao, M., Kim, E.Y., Zwart, P.H., Sankaran, B., Arthanari, H., Sousa, M.C., De Vivo, M., Fox, J.M., 2018. Abietane-type diterpenoids inhibit protein tyrosine phosphatases by stabilizing an inactive enzyme conformation. Biochemistry 57, 5886–5896. https://doi.org/10.1021/acs.biochem.8b00655.

International Diabetes Federation, 2019. IDF Diabetes Atlas, ninth ed. Brussels, Belgium. https://diabetesatlas.org/atlas/ninth-edition/.

Kjaerulff, L., Jensen, A.B.J., Ndi, C., Semple, S., Møller, B.L., Staerk, D., 2020. Isolation, structure elucidation and PTP1B inhibitory activity of serrulatane diterpenoids from the roots of *Myoporum insulare*. Phytochem. Lett. 39, 49–56. https://doi.org/10.1016/j.phytol.2020.07.001.

Kumar, R., Duffy, S., Avery, V.M., Carroll, A.R., Davis, R.A., 2018. Microthecaline A, a quinoline serrulatane alkaloid from the roots of the Australian desert plant *Eremophila microtheca*. J. Nat. Prod. 81, 1079–1083. https://doi.org/10.1021/acs.jnatprod.7b00992.

Luo, D., Callari, R., Hamberger, B., Wubshet, S.G., Nielsen, T.N., Andersen-Ranberg, J., Hallström, B.M., Cozzi, F., Heider, H., Møller, B.L., Staerk, D., Hamberger, B., 2016. In: Proc. Natl. Acad. Sci. U.S.A., vol. 113, pp. E5082–E5089. https://doi.org/10.1073/pnas.1607504113.

Ndi, C.P., Semple, S.J., Griesser, H.J., Pyke, S.M., Barton, M.D., 2007. Antimicrobial compounds from *Eremophila serrulata*. Phytochemistry 68, 2684–2690. https://doi.org/10.1016/j.phytochem.2007.05.039.

Newman, D.J., Cragg, G.M., 2020. Natural products as sources of new drugs over the nearly four decades from 01/1981 to 09/2019. J. Nat. Prod. 83, 770–803. https://doi.org/10.1021/acs.jnatprod.9b01285.

Padhi, S., Nayak, A.K., Behera, A., 2020. Type II diabetes mellitus: a review on recent drug based therapeutics. Biomed. Pharmacother. 131, 110708. https://doi.org/10.1016/j.biopha.2020.110708.

Pedersen, H.A., Ndi, C., Semple, S.J., Buirchell, B., Møller, B.L., Staerk, D., 2020. PTP1B-inhibiting branched-chain fatty acid dimers from *Eremophila oppositifolia* subsp. *angustifolia* identified by high-resolution PTP1B inhibition profiling and HPLC-PDA-HRMS-SPE-NMR analysis. J. Nat. Prod. 83, 1598–1610. https://doi.org/10.1021/acs.jnatprod.0c00070.

Pescitelli, G., Bruhn, T., 2016. Good computational practice in the assignment of absolute configurations by TDDFT calculations of ECD spectra. Chirality 28, 466–474. https://doi.org/10.1002/chir.22600.

Reinhardt, J.K., Klemd, A.M., Danton, O., De Mieri, M., Smiesko, M., Huber, R., Burgi, T., Grundemann, C., Hamburger, M., 2019. Sesquiterpene lactones from *Artemisia argyi*: absolute configuration and immunosuppressant activity. J. Nat. Prod. 82, 1424–1433. https://doi.org/10.1021/acs.jnatprod.8b00791.

Semple, S.J., Reynolds, G.D., O'Leary, M.C., Flower, R.L., 1998. Screening of Australian medicinal plants for antiviral activity. J. Ethnopharmacol. 60, 163–172. https://doi.org/10.1016/s0378-8741(97)00152-9.

Singab, A.N., Youssef, F.S., Ashour, M.L., Wink, M., 2013. The genus *Eremophila* (Scrophulariaceae): an ethnobotanical, biological and phytochemical review. J. Pharm. Pharmacol. 65, 1239–1279. https://doi.org/10.1111/jphp.12092.

Smith, J.E., Tucker, D., Watson, K., Jones, G.L., 2007. Identification of antibacterial constituents from the indigenous Australian medicinal plant *Eremophila duttonii* F. Muell. (Myoporaceae). J. Ethnopharmacol. 112, 386–393. https://doi.org/10.1016/j.jep.2007.03.031.

Tahtah, Y., Wubshet, S.G., Kongstad, K.T., Heskes, A.M., Pateraki, I., Møller, B.L., Jäger, A.K., Staerk, D., 2016. High-resolution PTP1B inhibition profiling combined with high-performance liquid chromatography–high-resolution mass spectrometry–solid-phase extraction–nuclear magnetic resonance spectroscopy: proof-of-concept and antidiabetic constituents in crude extract of *Eremophila lucida*. Fitoterapia 110, 52–58. https://doi.org/10.1016/j.fitote.2016.02.008.

Tomasi, J., Mennucci, B., Cammi, R., 2005. Quantum mechanical continuum solvation models. Chem. Rev. 105, 2999–3093. https://doi.org/10.1021/cr9904009.

Wang, L., Chen, K., Zhang, M., Ye, M., Qiao, X., 2021. Catalytic function, mechanism, and application of plant acyltransferases. Crit. Rev. Biotechnol. https://doi.org/10.1080/07388551.2021.1931015.

Wubshet, S.G., Tahtah, Y., Heskes, A.M., Kongstad, K.T., Pateraki, I., Hamberger, B., Møller, B.L., Staerk, D., 2016. Identification of PTP1B and α-glucosidase inhibitory serrulatanes from *Eremophila* spp. by combined use of dual high-resolution PTP1B and α-glucosidase inhibition profiling and HPLC-HRMS-SPE-NMR. J. Nat. Prod. 79, 1063–1072. https://doi.org/10.1021/acs.jnatprod.5b01128.

Zabolotny, J.M., Bence-Hanulec, K.K., Stricker-Krongrad, A., Haj, F., Wang, Y., Minokoshi, Y., Kim, Y.B., Elmquist, J.K., Tartaglia, L.A., Kahn, B.B., Neel, B.G., 2002. PTP1B regulates leptin signal transduction in vivo. Dev. Cell 2, 489–495. https://doi.org/10.1016/s1534-5807(02)00148-x.

Zahran, E.M., Abdelmohsen, U.R., Hussein, A.S., Salem, M.A., Khalil, H.E., Yehia Desoukey, S., Fouad, M.A., Kamel, M.S., 2019. Antiulcer potential and molecular docking of flavonoids from *Ocimum forskolei* Benth., family Lamiaceae. Nat. Prod. Res. 35, 1–5. https://doi.org/10.1080/14786419.2019.1645662.